

Nonlinear and ROADM induced penalties in 28 Gbaud dynamic optical mesh networks employing electronic signal processing

Danish Rafique* and Andrew D. Ellis

Photonics Systems Group, Tyndall National Institute and Department of Electrical Engineering/Physics,
University College Cork, Dyke Parade, Prospect Row, Cork, Ireland

*danish.rafique@tyndall.ie

Abstract: We report the impact of cascaded reconfigurable optical add-drop multiplexer induced penalties on coherently-detected 28 Gbaud polarization multiplexed m -ary quadrature amplitude modulation (PM m -ary QAM) WDM channels. We investigate the interplay between different higher-order modulation channels and the effect of filter shapes and bandwidth of (de)multiplexers on the transmission performance, in a segment of pan-European optical network with a maximum optical path of 4,560 km (80km x 57 spans). We verify that if the link capacities are assigned assuming that digital back propagation is available, 25% of the network connections fail using electronic dispersion compensation alone. However, majority of such links can indeed be restored by employing single-channel digital back-propagation employing less than 15 steps for the whole link, facilitating practical application of DBP. We report that higher-order channels are most sensitive to nonlinear fiber impairments and filtering effects, however these formats are less prone to ROADM induced penalties due to the reduced maximum number of hops. Furthermore, it has been demonstrated that a minimum filter Gaussian order of 3 and bandwidth of 35 GHz enable negligible excess penalty for any modulation order.

©2011 Optical Society of America

OCIS codes: (060.1660) Coherent communications; (060.4254) Networks, combinatorial network design; (060.4256) Networks, network optimization; (060.4370) Nonlinear optics, fibers.

References

1. A. D. Ellis, J. Zhao, and D. Cotter, "Approaching the non-linear Shannon limit," *J. Lightwave Technol.* **28**(4), 423–433 (2010).
2. R.-J. Essiambre, G. Kramer, P. J. Winzer, G. J. Foschini, and B. Goebel, "Capacity limits of optical fiber networks," *J. Lightwave Technol.* **28**(4), 662–701 (2010).
3. X. Liu, S. Chandrasekhar, B. Zhu, P. J. Winzer, A. H. Gnauck, and D. W. Peckham, "448-Gb/s reduced-guard-interval CO-OFDM transmission over 2000 km of ultra-large-area fiber and five 80-GHz-grid ROADMs," *J. Lightwave Technol.* **29**(4), 483–490 (2011).
4. D. Rafique, J. Zhao, and A. D. Ellis, "Digital back-propagation for spectrally efficient WDM 112 Gbit/s PM m -ary QAM transmission," *Opt. Express* **19**(6), 5219–5224 (2011).
5. S. Makovejs, D. S. Millar, V. Mikhailov, G. Gavioli, R. I. Killey, S. J. Savory, and P. Bayvel, "Experimental investigation of PDM-QAM16 transmission at 112 Gbit/s over 2400 km," in *Optical Fiber Communication Conference*, OSA Technical Digest (CD) (Optical Society of America, 2010), paper OMIJ6.
6. M. Nakazawa, S. Okamoto, T. Omiya, K. Kasai, and M. Yoshida, "256 QAM (64 Gbit/s) coherent optical transmission over 160 km with an optical bandwidth of 5.4 GHz," in *Optical Fiber Communication Conference*, OSA Technical Digest (CD) (Optical Society of America, 2010), paper OMIJ5.
7. G. Gavioli, E. Torrenco, G. Bosco, A. Carena, V. Curri, V. Miot, P. Poggiolini, M. Belmonte, A. Guglielame, A. Brinciotti, A. La Porta, F. Forghieri, C. Muzio, G. Osnao, S. Piciaccia, C. Lezzi, L. Molle, and R. Freund, "100Gb/s WDM NRZ-PM-QPSK long-haul transmission experiment over installed fiber probing non-linear reach with and without DCUs," in *35th European Conference on Optical Communication, 2009. ECOC '09* (2009), paper 3.4.2, pp. 1–2.
8. P. J. Winzer, A. H. Gnauck, S. Chandrasekhar, S. Draving, J. Evangelista, and B. Zhu, "Generation and 1,200-km transmission of 448-Gb/s ETDM 56-Gbaud PDM 16-QAM using a single IQ modulator," in *2010 36th European Conference and Exhibition on Optical Communication (ECOC)*, (2010), paper PD2.2, pp. 1–2.

9. X. Yi, N. K. Fontaine, R. P. Scott, and S. J. B. Yoo, "Tb/s coherent optical OFDM systems enabled by optical frequency combs," *J. Lightwave Technol.* **28**(14), 2054–2061 (2010).
10. A. Nag, M. Tornatore, and B. Mukherjee, "Optical network design with mixed line rates and multiple modulation formats," *J. Lightwave Technol.* **28**(4), 466–475 (2010).
11. C. Meusburger, D. A. Schupke, and A. Lord, "Optimizing the migration of channels with higher bitrates," *J. Lightwave Technol.* **28**(4), 608–615 (2010).
12. W. Wei, L. Zong, and D. Qian, "Wavelength-based sub-carrier multiplexing and grooming for optical networks bandwidth virtualization," in *National Fiber Optic Engineers Conference*, OSA Technical Digest (CD) (Optical Society of America, 2008), paper PDP35.
13. G. P. Agrawal, *Nonlinear Fiber Optics* (Academic Press, 2007).
14. M. S. Alfiad, M. Kuschnerov, T. Wuth, T. J. Xia, G. Wellbrock, E. D. Schmidt, D. van den Borne, B. Spinnler, C. J. Weiske, E. de Man, A. Napoli, M. Finkenzeller, S. Spaelter, M. Rehman, J. Behel, M. Chbat, J. Stachowiak, D. Peterson, W. Lee, M. Pollock, B. Basch, D. Chen, M. Freiburger, B. Lankl, and H. de Waardt, "111-Gb/s transmission over 1040km field-deployed fiber with 10/40G neighbors," *Photonics Technol. Lett.* **21**(10), 615–617 (2009).
15. T. Wuth, M. W. Chbat, and V. F. Kamalov, "Multi-rate (100G/40G/10G) transport over deployed optical networks," in *National Fiber Optic Engineers Conference*, OSA Technical Digest (CD) (Optical Society of America, 2008), paper NTuB3.
16. D. Rafique and A. D. Ellis, "Nonlinear penalties in long-haul optical networks employing dynamic transponders," *Opt. Express* **19**(10), 9044–9049 (2011).
17. E. Ip, "Nonlinear compensation using backpropagation for polarization-multiplexed transmission," *J. Lightwave Technol.* **28**(6), 939–951 (2010).
18. L. B. Du and A. J. Lowery, "Improved single channel backpropagation for intra-channel fiber nonlinearity compensation in long-haul optical communication systems," *Opt. Express* **18**(16), 17075–17088 (2010).
19. D. Rafique, M. Mussolin, M. Forzati, J. Mårtensson, M. N. Chugtai, and A. D. Ellis, "Compensation of intra-channel nonlinear fibre impairments using simplified digital back-propagation algorithm," *Opt. Express* **19**(10), 9453–9460 (2011).
20. L. Li, Z. Tao, L. Dou, W. Yan, S. Oda, T. Tanimura, T. Hoshida, and J. C. Rasmussen, "Implementation efficient nonlinear equalizer based on correlated digital backpropagation," in *Optical Fiber Communication Conference*, OSA Technical Digest (CD) (Optical Society of America, 2011), paper OWW3.
21. E. Ip, N. Bai, and T. Wang, "Complexity versus performance tradeoff in fiber nonlinearity compensation using frequency-shaped, multi-subband backpropagation," in *Optical Fiber Communication Conference*, OSA Technical Digest (CD) (Optical Society of America, 2011), paper OThF4.
22. L. Zhu and G. Li, "Folded digital backward propagation for dispersion-managed fiber-optic transmission," *Opt. Express* **19**(7), 5953–5959 (2011).
23. T. Otani, N. Antoniadis, I. Roudas, and T. E. Stern, "Cascadability of passband-flattened arrayed waveguide-grating filters in WDM optical networks," *Photonics Technol. Lett.* **11**(11), 1414–1416 (1999).
24. F. Heismann, "System requirements for WSS filter shape in cascaded ROADMs networks," in *Optical Fiber Communication Conference*, OSA Technical Digest (CD) (Optical Society of America, 2010), paper OThR1.
25. M. Filer and S. Tibuleac, "DWDM transmission at 10Gb/s and 40Gb/s using 25GHz grid and flexible-bandwidth ROADMs," in *National Fiber Optic Engineers Conference*, OSA Technical Digest (CD) (Optical Society of America, 2011), paper NThB3.
26. Y. Levy and M. Shtaf, "The effect of strong inline filtering on the amplitude jitter in long optical systems," *J. Lightwave Technol.* **24**(8), 3097–3102 (2006).
27. M. Borgne, "Comparison of high-level modulation schemes for high-capacity digital radio systems," *IEEE Trans. Commun.* **33**(5), 442–449 (1985).
28. P. Mathiopoulos and K. Feher, "Performance evaluation of a 512-QAM system in distorted channels," *IEE Proc. F Commun. Radar Signal Proc.* **133**(2), 199–204 (1986).
29. D. Rafique, J. Zhao, and A. D. Ellis, "Compensation of nonlinear fibre impairments in coherent systems employing spectrally efficient modulation formats," *IEICE Transactions on Communications*, **E 94-B**(7), 1815–1822 (2011).
30. K. Roberts, "Digital signal processing for coherent optical communications: current state of the art and future challenges," in *Signal Processing in Photonic Communications*, OSA Technical Digest (CD) (Optical Society of America, 2011), paper SPWC1.

1. Introduction

The growing demand for high-bandwidth digital multimedia applications continues to increase the capacity requirements of optical transmission systems [1,2]. The spectral efficiency has become one of the most critical tools for increasing the transmission capacity of optical networks, and has led to considerable research activity in advanced modulation formats employing coherent detection [3,4]. In particular, polarization multiplexed m -ary quadrature amplitude (PM-mQAM) modulation formats have received tremendous attention with reference to next-generation network upgrades [5,6], and at present, research is focused on developing wavelength-division-multiplexed (WDM) networks having per-channel data rates of 100 Gb/s and beyond [7–9]. The ability to deploy a dynamic and configurable optical

layer is a direct consequence of such developments. This is particularly true for shorter links across the network, where the improved optical signal-to-noise ratio (OSNR) would allow the use of a high capacity channel. In dynamic optical networks, there is a large range of variables to provide the desired flexibility, including symbol rate [10,11], sub-carrier modulation [12] and signal constellation [4], however, symbol rate and sub-carrier modulation would require modification of the existing reconfigurable add drop multiplexer (ROADM) based infrastructure.

While such dynamic networks enable flexible capacity allocation, these systems present complex trade-offs. One such challenge is associated with the nonlinear transmission impairments [10–13]. In particular, it has been reported recently that the upgrade of a wavelength channel to a high spectral efficiency format is constrained by nonlinear cross-talk from the other network traffic [14–16], especially if the reach is such that intra-channel nonlinearities degrading the higher bit-rate traffic (e.g. 400 Gb/s) require mitigation by the use of digital back-propagation (DBP) [17–19]. Although the future potential of nonlinear impairment compensation using DBP in a dynamic optical network is unclear due to its significant computational burden and limited access to the full dense wave-division multiplexing band, simplification of nonlinear DBP algorithm using single-channel processing at the receiver has already commenced [18–22]. Another challenge arises from transmission penalties due to ROADM cascades, which have been identified as one of the most critical limiting factors in 50GHz-spaced WDM systems [23–25], and will also be a factor in grid-less networks. This can impose strict requirements on the flexibility and filter selection criteria for networks, and limit the number of optical nodes that can be cascaded. Consequently, it is of great importance to know the number and/or type of filters that a signal traverses and their impact on nonlinear transmission performance [26–28].

In this paper we focus on flexibility in the signal constellation, allowing for evolution of the existing ROADM based network. We consider a configuration where network capacity is increased by introducing higher-order modulation traffic routes selected from design rules based on digital nonlinearity compensation methods in a coherently-detected 28 Gbaud PM-mQAM network architecture. We demonstrate that even if route-lengths are chosen based on this knowledge of the physical layer limitations of the added channel after single-channel digital back-propagation, for the network studied, the majority of the network connections (75%) are operable with significant OSNR margin with electronic dispersion compensation alone. However, 25% of the remaining links require the use of single-channel DBP for error free operation. Furthermore, we demonstrate that in this network higher-order modulation formats are more prone to impairments due to channel nonlinearities and filter crosstalk; however they are less affected by the bandwidth constriction associated with ROADM cascades due to shorter operating distances. Finally, we show that, for any given modulation order, a minimum filter Gaussian order of ~ 3 or bandwidth of ~ 35 GHz enables the performance with approximately less than 1 dB penalty with respect to ideal rectangular filters.

2. System configuration

Figure 1 illustrates the simulation setup. The optical network comprised 28 Gbaud WDM channels, employing PM-mQAM (m : 4, 16, 64) formats with a channel spacing of 50 GHz, a series of optical network nodes spaced according to a particular route of a Pan-European network (see Fig. 2), but with the node spacing set to the nearest 80km, allowing for uniformly spaced amplifiers. For all the carriers, at all of the nodes, both the polarization states were modulated independently using de-correlated 2^{15} and 2^{16} pseudo-random bit sequences (PRBS) with different random number seeds, for x- and y-polarization states, respectively. Each PRBS was de-multiplexed separately into two multi-level output symbol streams which were used to modulate an in-phase and a quadrature-phase carrier. The optical transmitters consisted of continuous wave laser sources (5 kHz line-width), followed by two nested Mach-Zehnder Modulator structures for x- and y-polarization states, and the two polarization states were combined using an ideal polarization beam combiner. The simulation

conditions ensured 16 samples per symbol with 2^{13} total simulated symbols per polarization, and the average power of all the channels was set to be equal.

The signals were multiplexed, and propagated over a standard single mode fiber transmission link with 80 km spans, no inline dispersion compensation and single-stage erbium doped fiber amplifiers (EDFAs). Each amplifier stage was modeled with a 4.5 dB noise figure and the total amplification gain was set to be equal to the total loss in each span. See Table 1 for simulation parameters. At the coherent receiver the signals were pre-amplified, de-multiplexed, coherently-detected using four balanced detectors to give the baseband electrical signal and sampled at 2 samples per symbol. Transmission impairments were digitally compensated in two scenarios. Firstly electronic compensation was applied via single-channel DBP (SC-DBP), which was numerically implemented by up-sampling the received signal to 16 samples/symbol and reconstructing the optical field from the in-phase and quadrature samples, followed by split-step Fourier method based solution of the nonlinear Schrödinger equation. Note that we initially considered a high number of samples per symbol to enable high DBP precision, however it has been shown previously that similar performance may be achieved with only 2 samples/symbol [29]. Unless mentioned otherwise, the upper bound on the step-size was set to be 1 km and the step length was chosen adaptively during the integration along the fiber based on the condition that in each step the nonlinear effects must change the phase of the optical field by no more than 0.05 degrees. In context of recent efforts for simplification of DBP algorithms, e.g., [20], for those connections which would benefit from DBP, we also employed a simplified DBP algorithm similar to [19], with number of steps varying from 0.5 step/span to 2 steps/span. In the second case electronic dispersion compensation (EDC) was used, and the back-propagation section in Fig. 1 was bypassed; finite impulse response (FIR) filters (T/2-spaced taps) adapted using a least mean square algorithm were employed. Polarization de-multiplexing and residual dispersion compensation was then performed using FIR filters, which was followed by carrier phase recovery. Finally, the symbol decisions were made and the performance assessed by direct error counting (converted into an effective Q-factor (Q_{eff})). The results were also plotted in terms of required OSNR (OSNR_R) at a BER of 3.8×10^{-3} (Q_{eff} of approximately 8.5 dB) calculated by receiver noise loading. All the numerical simulations were carried out using VPItransmissionMaker®v8.5, and the digital signal processing was performed in MATLAB®7.10.

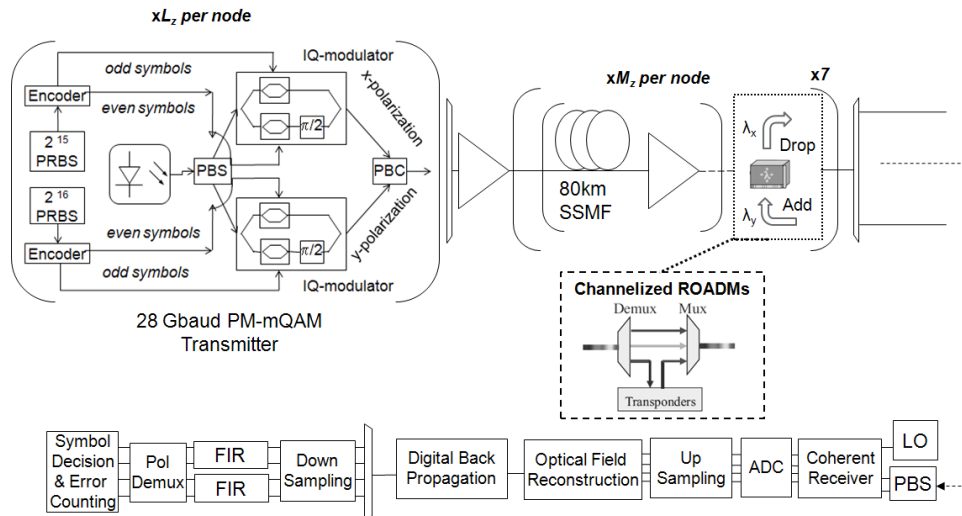


Fig. 1. Simulation setup for 28 Gbaud Gb/s PM-mQAM ($m = 4, 16, 64$) transmission system with L wavelengths and M spans per node, where z represents the node number.

To establish a preliminary estimate of maximum potential transmission distance of each available format, we employed the transmission reaches identified in [16]. These are suitable to enable a BER of 3.8×10^{-3} at a fixed launch power of -1 dBm assuming the availability of single-channel DBP. These conditions gave maximum reaches of 2,400 km for PM-16QAM, 640 km for PM-64QAM and 160 km for 256 QAM, leading to the link allocation shown in Table 1. Note that only SC-DBP was considered in this study since in a realistic mesh network access to neighboring traffic might be impractical. WDM based DBP solution may be suitable for a point to point submarine link or for a network connection where wavelengths linking the same nodes co-propagate using adjacent wavelengths. Implementation of this condition would require wide band DBP aware routing and wavelength assignment algorithms. This approach could enable significant Q_{eff} improvements or reach increases. For 64QAM, up to 7dB Q_{eff} improvements were shown in [4], although the benefit depends on the number of processed channels [29].

Table 1. Parameters and Distance Constraints

Baud-rate (Gbaud)	Dispersion (ps/nm/km)	Loss (dB/km)	Nonlinearity (1/W/km)	Wavelengths	Channel spacing
28	20	0.2	1.5	20	50 GHz
Filter (GHz)			Modulation formats and distance constraints		
Type: Gauss./Rect., BW: 25-45			4QAM (≥ 31 spans), 16QAM (≥ 9 spans), 64QAM (≥ 3 spans), 256QAM (≥ 1 spans)		

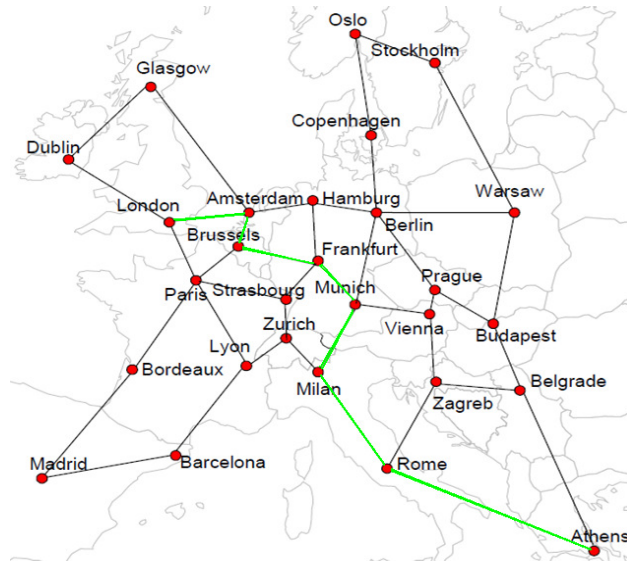


Fig. 2. 28-node Pan-European network topology. Link 1: London-to-Amsterdam, 7 spans, Link 2: Amsterdam-to-Brussels, 3 spans, Link 3: Brussels-to-Frankfurt, 6 spans. Link 4: Frankfurt-to-Munich, 6 spans, Link 5: Munich-to-Milan, 7 spans, Link 6: Milan-to-Rome, 9 spans, Link 7, Rome-to-Athens: 19 spans (80 km/span).

We then applied this link capacity rule to an 8-node route from a Pan-European network topology (see highlighted link in Fig. 2). To generate a traffic matrix, for each node, commencing with London, we allocated traffic from that node to all of the subsequent nodes, operating the link at the highest order constellation permissible for the associated transmission distance (Table 1). We note that none of the links in this chosen route were suitable for 256QAM, indeed only the Strasberg to Zurich and Vienna to Prague links are expected to be suitable for this format. Nevertheless, we selected the available wavelength nearest to the centre wavelength for each link. Once all nodes were connected by a single link, this process was repeated (in the same order), adding additional capacity between nodes where an unblocked route was available until all 20 wavelengths were allocated, and no more traffic

could be assigned without blockage. Table 2 illustrates the resultant traffic matrix showing the location where traffic was added and dropped (gray squares) and the order of the modulation format emerging from that node on each wavelength (numbers) as a function of the link number (vertical) and wavelengths (horizontal). For example, emerging from node 6 are nine wavelengths carrying PM-4QAM and 5 wavelengths carrying PM-16QAM whilst on the centre wavelength, PM-16QAM data is transmitted from node 1 (London) to node 5 (Munich) where this traffic is dropped and replaced with PM-64QAM traffic destined for node 6 (Milan). This ensured that various nodes were connected by multiple wavelengths. As it can be seen, the adopted procedure allowed for a reasonably meshed optical network (36 connections) with shortest route of 3 spans and longest path of 57 spans, emulating a quasi-real traffic scenario. At each node, add-drop functionality was enabled using a channelized ROADM architecture where all the wavelengths were de-multiplexed and channels were added/dropped, before re-multiplexing the data signals again. This is shown in Fig. 1. We considered Rectangular and Gaussian-shaped filters for ROADM stages, and the order of the Gaussian filters was varied from 1 through 6.

Table 2. Traffic Matrix (Each Element Represents the Modulation Order; Traffic Dropped and Added at Nodes Highlighted in Gray)

X(λ)	-	-	-	-	-	-	-	-	-	-	0	+	+	+	+	+	+	+	+		
Y (Link)	10	9	8	7	6	5	4	3	2	1		1	2	3	4	5	6	7	8	9	
1	4	16	16					64	4	16	16	4	64		16	16	16			16	4
2	4	16	16	16	64	64	4	16	4	16	16	4	16	4	16	16	16			16	4
3	4	16	16	16	4	16	4	16	4	16	16	4	16	4	16	16	16	64		16	4
4	4	16	4	16	4	16	4	16	4	16	16	4	16	4	16	16	64	16		16	4
5	4	16	4	16	4	16	4	16	4	16	64	4	16	4	4	16			16		4
6	4		4		4		4	4	16	16		4	16	4	4	16			16		4
7	4		4		4		4	4	16	16					4						

3. Results and discussions

3.1 Nonlinear transmission (ideal ROADMs)

Figure 3 depicts the required OSNR ($OSNR_R$) of each network connection as a function of transmission distance, after EDC. Note that in this case we employed rectangular ROADM filters to isolate the impact of inter-channel nonlinear impairments from filtering crosstalk (no cascade penalties were observed with ideal filters). Numerous conclusions can be ascertained from this figure. First, these results confirm that with mixed-format traffic and active ROADMs, as the transmission distance is increased the $OSNR_R$ increases irrespective of the modulation order due to channel nonlinearities. Second, we confirm that the higher-order channels are most degraded by channel nonlinearities, even at the shortest distance traversed, and the offset between the theoretical OSNR for a linear system and the simulated values are greater for such formats. This is attributed to the significantly reduced minimum Euclidian distance which leads to increased sensitivity to nonlinear effects [4]. However, for a system designed according to SC-DBP propagation limits, as the one studied here, one can observe that majority of the links operate using EDC alone (except the ones highlighted by up-arrows). Note that managing the peak-to-average power ratio for such formats through linear pre-distortion could improve the transmission performance, as shown in [16]. Additionally, in order to examine the available system margin, Fig. 3 also shows the received OSNR for various configurations, where it can be seen that majority of the links (except 3) have more than 2 dB available margins, and that our numerical results show an excellent match to the theoretical predictions.

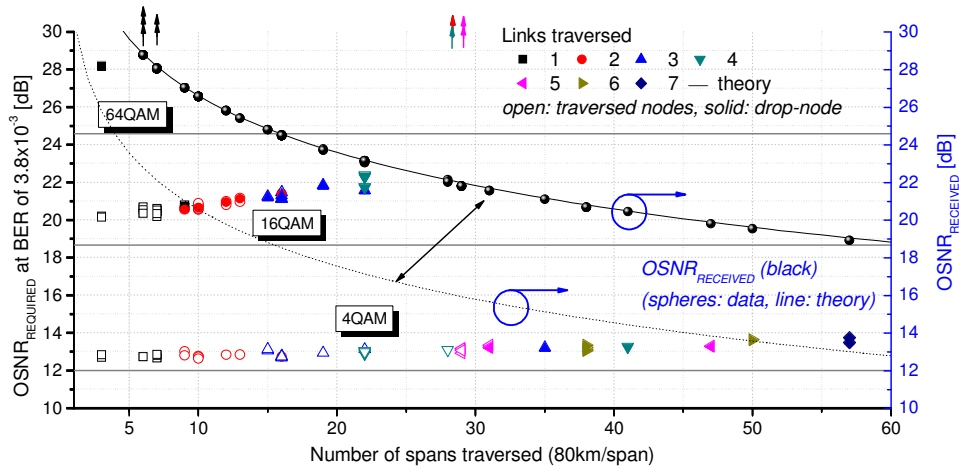


Fig. 3. Nonlinear tolerance of PM-mQAM in a dynamic mesh network after EDC. a) Colored: $OSNR_R$ at BER of 3.8×10^{-3} vs. Distance (Links traversed: 1(square), 2(circle), 3(up-tri), 4(down-tri), 5(left-tri), 6(right-tri), 7(diamond), horizontal lines (theoretical $OSNR_{REQUIRED}$)), open: intermediate nodes, solid: destination nodes. Black: Received OSNR (black spheres), Line (theoretical received OSNR), Dotted Line (theoretical received OSNR with 5 dB margin). Up arrows indicate failed connections (corresponding to drop nodes)

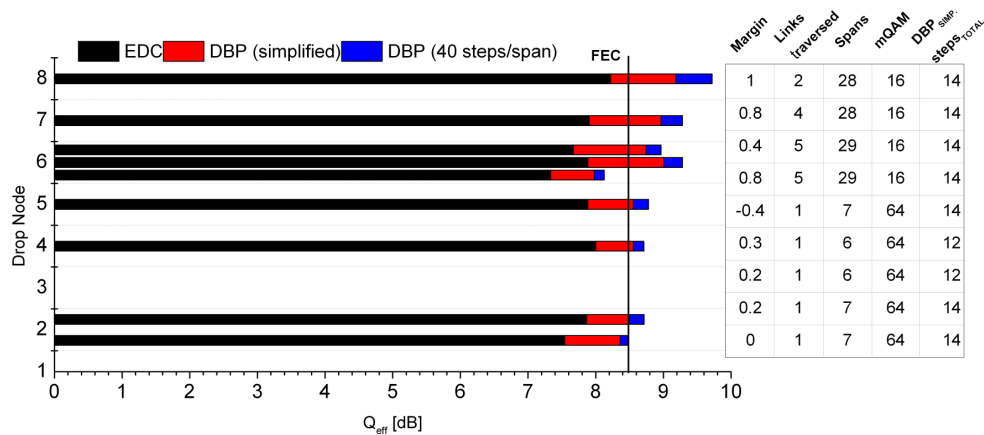


Fig. 4. Q_{eff} as a function of network nodes for failed routes, shown by up-arrows in Fig. 5, for PM-mQAM in a dynamic mesh network. After EDC (black) and single-channel DBP (red: simplified, blue: full-precision 40 steps/span). Table shows the network parameters for each scenario and number of steps for simplified DBP.

As discussed, the results presented in Fig. 3 exclude 9 network connections classified as failed (25% of the total traffic), where the calculated BER was always found to be higher than the FEC threshold (BER of 3.8×10^{-3}). In order to address the failed routes, we employed single-channel DBP on such channels, as shown in Fig. 4 (red: simplified, blue: full-precision 40 steps per span). It can be seen that all but one of the links can be restored given only single-channel DBP is employed, with the Q_{eff} increasing by an average of ~ 1 dB, consistent with the improvements observed for heterogeneous traffic [16]. Uniquely, the failed link (after SC-DBP) is operated with the highest order modulation format studied, and its two nearest neighbors are both highly dispersed. Note that even though the maximum node lengths are chosen based on nonlinear transmission employing single-channel DBP, most of the network traffic abide by the EDC constraints (64QAM: ≥ 1 span, 16QAM: ≥ 6 spans, 4QAM ≥ 24 spans). The failed links have one-to-one correlation with violation of EDC constraints, where

a quarter of total network traffic requires the implementation of single-channel DBP. Also, note that all but two of the links are operable with less than 15 steps for the whole link. These results give some indication of the benefit of flexible formats and DBP. For particular network studied (assuming one of the two failed links works with high precision DBP), if homogeneous traffic, employing 4QAM, is considered, a total network capacity of 4 Tb/s can be achieved. On the other hand, flexible m -ary QAM employing bandwidth allocation based on EDC performance limits (not shown) enables $\sim 60\%$ increase in transmission capacity (6.8 Tb/s), while designs accounting for SC-DBP add a further 12% increase in capacity (7.7 Tb/s). Note that for traffic calculations based on EDC constraints, we assumed that the routes of Fig. 4 would operate satisfactorily for the next format down. Further increase in capacity can be attained if pre-compensation [16] or WDM DBP [4] are used, or if more format granularity is introduced (e.g. 8QAM and 32QAM) to exploit the remaining margin. In this example, 25% of transponders operating in DBP mode enable a 12% increase in capacity. One may therefore argue that in order to provide a the same increase in capacity without employing DBP, approximately 12% more channels would be required, consuming 12% more energy (assuming that the energy consumption is dominated by the transponders). In the case studied, since a $\frac{1}{4}$ of transponders require DBP, breakeven would occur if the energy consumption of a DBP transponder was 50% greater than a conventional transponder. Given that commercial systems allocate approximately 3-5% of their power to the EDC chipset [30], this suggests that the DBP unit used could be up to 16 times the complexity of the EDC chip. The results reported in Fig. 4 with simplified DBP fall within this bound and highlight the practicality of simplified DBP algorithms.

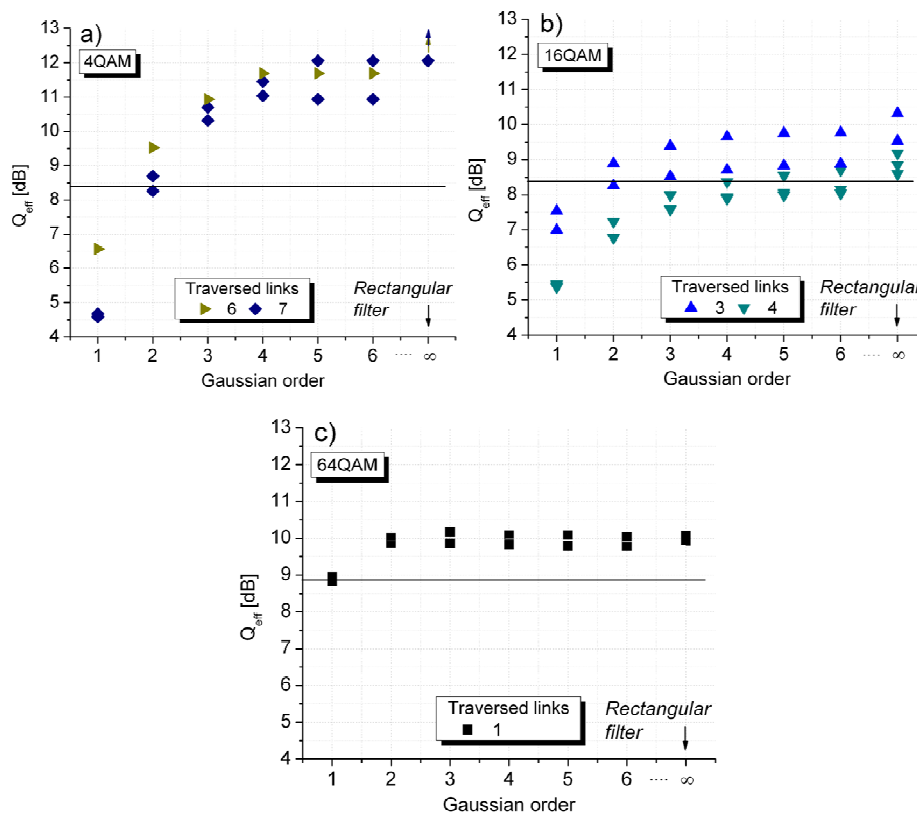


Fig. 5. Q_{eff} as a function of Gaussian filter order (35 GHz bandwidth) for a 6 dB margin from theoretical achievable OSNR. a) 4QAM; b) 16QAM; c) 64QAM. (up-arrows indicate that no errors were detected)

3.2 Nonlinear transmission as a function of filter order and bandwidth

Figure 5 shows the performance of a selection of links with less than 6 dB margin from the theoretical achievable OSNR (see Fig. 3 for links used, we show only the links with the worst OSNR_R in the case of 16QAM for clarity), as a function of the Gaussian filter order within each ROADM. As it is well-known, the transmission penalty decreases as filter order increases [24]. However, it can be seen that for higher-order modulation formats, the transmission performance saturates at lower filter orders, compared to lower-order formats. This trend is related to the fact that modulation formats traversing through greater number of nodes are strongly dependent on the Gaussian order (attributed to known penalties from filter cascades [23–25]). For instance, the performance of 4QAM traffic is severely degraded as a function of Gaussian order, due to the higher number of nodes traversed by such format. 16QAM channels show relatively good tolerance to filter order due to reduced number of hops, however when greater than 3 nodes are employed, the performance again becomes a strong function of filter order. 64QAM is least dependent on filter order since no intermediate ROADMs are traversed. For any given modulation order, a minimum Gaussian order of ~3 enables the optimum performance to be within 1 dB of the performance for an ideal rectangular filter.

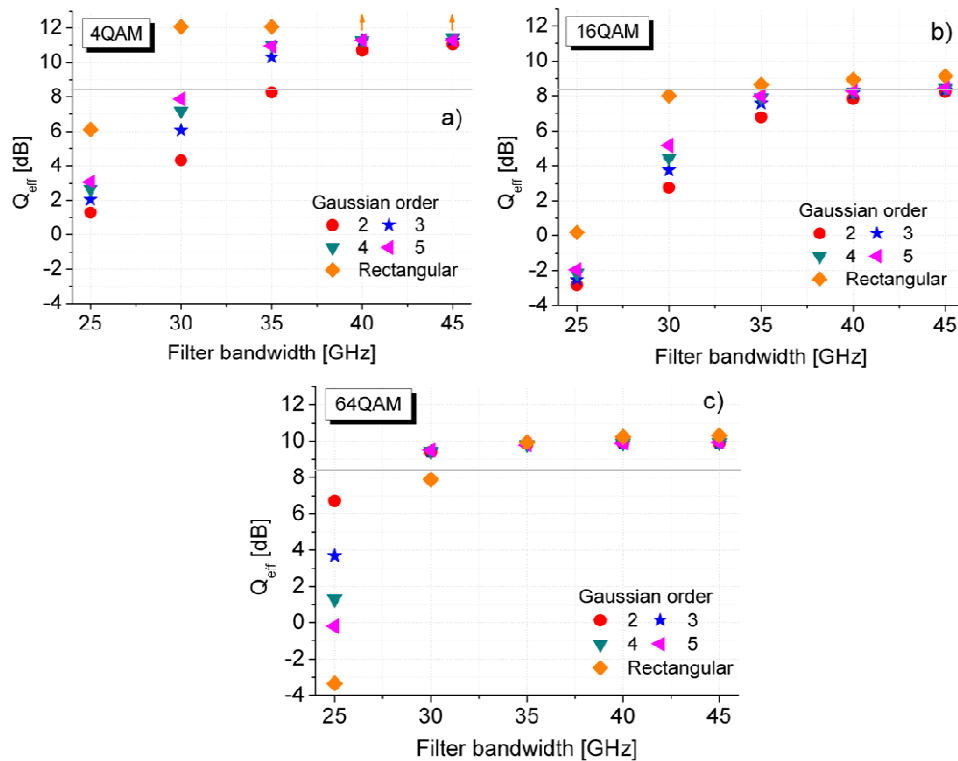


Fig. 6. Q_{eff} as a function of Gaussian filter bandwidth (and filter order) for worst-case OSNR margin seen in Fig. 5. a) 4QAM; b) 16QAM; c) 64QAM.

In the previous sections, we investigated the impact of filter shape and nonlinear fiber impairments on transmission performance. In order to verify these effects, we explore the added impact of filter bandwidth on system performance. The simulated Q_{eff} versus 3 dB bandwidth of the ROADM stages and filter order is shown in Fig. 6, for the worst-case OSNR_R observed in Fig. 3 for each modulation format. For lower bandwidths, the Q_{eff} is degraded due to bandwidth constraints. For higher bandwidths, since the filtering action of the coherent receiver eliminates linear crosstalk, the performance stabilizes. With the exception of

second order filters, bandwidths down to 35 GHz are sufficient for all the formats studied. However, consistent with previous analysis (in Fig. 5), the impact of filter order on 64QAM is minimal and lower-order filters seem to have better performance than higher-order ones at 25GHz bandwidth. This is because when the signal bandwidth (28 GHz) exceeds the filter bandwidth, the lower order filters capture more of the signal spectra. However, this effect is visible in the case of 64QAM only since no nodes were traversed in this case, thereby avoiding the penalty from ROADM stages with lower filter orders.

4. Conclusions

We have reported that if the traffic flows in a dynamic format network are allocated according to transmission distance constraints assuming the availability of digital back-propagation, a significant fraction (75% in our example) operate satisfactorily with only electronic dispersion compensation enabled. Operating the remaining channels with SC-DBP increases the overall network capacity to a certain extent (12% in this case) at the expense of additional power consumption in those transponders. For a network design constrained by the energy consumption per bit our results suggest that DBP is favorable provided that a DBP-based transponder consumes less than around 1.5 times the power of a standard EDC-based transponder., and we further confirm that simplified DBP enables tolerable complexity compared to EDC based transponders for commercial systems. Also we show that for any given modulation order, a minimum filter Gaussian order of 3 and with bandwidth of 35 GHz enables the performance with approximately less than 1 dB penalty with respect to ideal rectangular filters, and that the reduced reach of higher order formats significantly reduces the impact of ROADM-induced filtering penalties.

Acknowledgments

This work was supported by Science Foundation Ireland under Grant numbers 06/IN/I969 and 10/CE/I1853.